Energy-Band Structure and Optical Spectrum of Grey Tin*

Fred H. Pollak, Manuel Cardona, and C. W. Higginbotham†
Department of Physics, Brown University, Providence, Rhode Island 02912
and
Frank Herman and John P. Van Dyke‡
IBM Research Laboratory, San Jose, California 95114
(Received 2 December 1969)

A first-principles relativistic orthogonalized-plane-wave calculation has been used to determine the energy eigenvalues of grey tin at seven key points of the reduced zone. An extended zone $\vec{k}\cdot\vec{p}$ method has been used as an interpolation scheme to map out the band structure in the remainder of the zone. Optical constants and derivative optical constants have been calculated from the $\vec{k}\cdot\vec{p}$ parameters. The calculated normal incidence reflectivity is compared to experiment. A detailed critical-point analysis of the calculated optical spectra is presented. Valence-band mass parameters, effective masses, and g factors at several points in the zone have been obtained and are compared to available experimental data.

I. INTRODUCTION

The extended zone $\vec{k}\cdot\vec{p}$ method has been used with considerable success to investigate the band structure of several diamond- and zinc-blende-type semiconductors.[1-6] These detailed band structures represent the starting point of calculations of optical constants[6,7] which provide insight into the relationship between the band structure and the characteristic features of the optical spectrum. In the $\vec{k}\cdot\vec{p}$ method,[1-3] the energy-band structure is determined by a set of parameters which represent energy gaps at $\vec{k}=0$, momentum matrix elements, and spin-orbit coupling strengths. While it is a straightforward matter to work out the energy-band structure at a large number of points in the reduced zone once a set of parameters has been chosen, it requires considerable effort and skill to arrive at a satisfactory set of parameters.

In most applications it is possible to determine experimentally some of the key parameters, and to estimate many of the others. Some estimates can be obtained from rough interpretations of experiment; others can be arrived at by using the results of the first-principles (as opposed to empirical) energy-band calculations. While considerable progress has already been made by using parameters whose values have been obtained from various different sources, it seems desirable to consider a band structure all of whose parameters have been determined on the same basis. Brinkman and Goodman have used the full-zone $\vec{k}\cdot\vec{p}$ method as an interpolation scheme in conjunction with an orthogonalized-plane-wave (OPW) calculation for Si.[8] Buss and Parada[9] have recently used the $\vec{k}\cdot\vec{p}$ method to calculate the optical constants of PbTe. The $\vec{k}\cdot\vec{p}$ parameters (energy gaps and matrix elements of $\vec{p}$) were determined from the augmented-plane-wave (APW) eigenvalues and eigenvectors at $\vec{k}=0$.

In the present paper we discuss an energy-band calculation for grey tin (α-Sn) which makes use of first-principles relativistic OPW results to establish the energy levels at selected high-symmetry points in the reduced zone, and of $\vec{k}\cdot\vec{p}$ results to map out the band structure in the remainder of the zone. All of the parameters appearing in the $\vec{k}\cdot\vec{p}$ interpolation scheme are obtained by requiring this scheme to reproduce the first-principles results at several points in the reduced zone. Thus all of the $\vec{k}\cdot\vec{p}$ parameters are determined on the same basis. In addition to the higher degree of internal consistency made possible by this procedure, the large number of energy levels available for fitting (over 60 at seven widely separated points of the reduced zone) enables us to remove restrictive assumptions used in previous $\vec{k}\cdot\vec{p}$ calculations. Prominent among those assumptions is the existence of only one independent matrix element of the spin-orbit interaction forced by the scarcity of experimental data.

The imaginary part of the dielectric constant, $\epsilon_2(\omega)$, has been calculated from the $\vec{k}\cdot\vec{p}$ parameters using a method originated by Gilat *et al.*[10] for calculating phonon spectra, and adapted for application to electronic spectra by the present authors.[6,7,11] The Kramers-Kronig relations were used to obtain the real part of the dielectric constant, $\epsilon_1(\omega)$. The normal incidence reflectivity spectrum $R(\omega)$ was obtained from $\epsilon_1(\omega)$ and $\epsilon_2(\omega)$ and compared to experimental results.[12] A detailed critical-point analysis of the calculated optical spectra is prosecuted. A survey of all existing experimental data for α-Sn and the corresponding calculated values is given.

TABLE I. OPW and $\vec{k}\cdot\vec{p}$ energy levels for α-Sn. All energies are in eV and the units of $\vec{k}$ are $2\pi/\alpha$, where α is the lattice constant. The symmetry classification is based on the notation of Ref. 17. The single group notation is indicated in parenthesis. The zero of energy has been placed at the Γ_8^+ level.

Level	OPW	$\vec{k}\cdot\vec{p}$	Level	OPW	$\vec{k}\cdot\vec{p}$	Level	OPW	$\vec{k}\cdot\vec{p}$
	$\vec{k}=(0,0,0)$			$\vec{k}=(\frac{1}{4},\frac{1}{4},\frac{1}{4})$			$\vec{k}=(\frac{1}{2},\frac{1}{2},\frac{1}{2})$	
$(\Gamma_{2'}^{u})$		10.40	Uncertain	6.86	6.73	Uncertain	8.84	9.19
$(\Gamma_{25'}^{u})$		9.87	Λ_6 (Λ_1)	6.53	6.67	L_6^+ (L_1)	8.25	8.72
Γ_8^- $(\Gamma_{12'})$	7.79	7.80	Λ_6 (Λ_1)	4.45	4.50	L_6^- $(L_{2'})$	5.94	6.37
Γ_6^+ (Γ_1^u)	5.16	5.18	$\Lambda_{4,5c}$ (Λ_3)	3.25	3.32	$L_{4,5c}^+$ (L_3)	3.43	3.39
Γ_8^- (Γ_{15})	2.43	2.43	Λ_{6c} (Λ_3)	2.95	3.00	L_{6c}^+ (L_3)	3.21	3.25
Γ_6^- (Γ_{15})	1.95	1.96	Λ_{6c} (Λ_1)	0.52	0.51	L_{6c}^+ (L_1)	0.15	0.17
Γ_8^+ $(\Gamma_{25'}^l)$	0.00	0.00	$\Lambda_{4,5v}$ (Λ_3)	−0.63	−0.59	$L_{4,5v}^-$ $(L_{3'})$	−0.98	−0.97
Γ_7^- $(\Gamma_{2'}^l)$	−0.416	−0.416	Λ_{6v} (Λ_3)	−1.05	−1.02	L_{6v}^- $(L_{3'})$	−1.39	−1.41
Γ_7^+ $(\Gamma_{25'}^l)$	−0.654	−0.654	Λ_6 (Λ_1)	−4.06	−4.00	L_6^+ (L_1)	−6.28	−6.42
Γ_6^+ (Γ_1^l)	−10.59	−10.59	Λ_6 (Λ_1)	−10.03	−10.03	L_6^- $(L_{2'})$	−9.07	−8.89
	$\vec{k}=(\frac{1}{2},0,0)$			$\vec{k}=(1,0,0)$			$\vec{k}=(\frac{1}{2},\frac{1}{2},0)$	
Δ_6 (Δ_1)	8.07	8.26	X_5 (X_1)	9.18{	11.36	Σ_5 (Σ_1)	7.63	9.30
Δ_7 $(\Delta_{2'})$	5.77	5.12			9.25	Σ_5 (Σ_2)	6.33	5.87
Δ_7 (Δ_5)	4.72	4.94	X_5 (X_3)	7.69{	9.19	Σ_5 (Σ_3)	4.44	4.82
Δ_6 (Δ_5)	4.70	4.85			8.87	Σ_5 (Σ_1)	4.07	4.10
Δ_{7c} $(\Delta_{2'})$	2.32	2.55	X_{5c} (X_1)	0.97	0.96	Σ_5 (Σ_4)	3.99	3.98
Δ_{6c} (Δ_1)	1.10	1.09	X_{5v} (X_4)	−2.43	−2.43	Σ_{5c} (Σ_3)	1.70	1.56
Δ_{6v} (Δ_5)	−1.59	−1.61	X_5 (X_1)	−7.59	−7.59	Σ_{5v} (Σ_2)	−1.29	−1.20
Δ_{7v}^* (Δ_5)	−1.72	−1.71				Σ_{5v} (Σ_1)	−2.95	−2.92
Δ_7 $(\Delta_{2'})$	−4.20	−4.15				Σ_5 (Σ_3)	−5.61	−5.54
Δ_6 (Δ_1)	−9.82	−9.83				Σ_5 (Σ_1)	−9.16	−9.14
	$\vec{k}=(1,\frac{1}{2},0)$			Core states				
(W_2)	8.90	13.16	$4d_{5/2}$	−19.6				
(W_2)	8.61	10.23	$4d_{3/2}$	−20.6				
(W_2)	4.03	9.14						
(W_2)	3.99	3.95						
(W_1)	3.66	3.82						
(W_1)	3.35	3.62						
(W_2)	−2.87	−2.93						
(W_2)	−3.04	−3.10						
(W_1)	−7.49	−7.28						
(W_1)	−7.55	−7.56						

II. OPW AND $\vec{k}\cdot\vec{p}$ ENERGY BANDS

A. OPW Energy Bands

The starting point of the present work was a relativistic OPW energy-band calculation based on a simplified but physically realistic crystal potential. This crystal potential had the form of a spatial superposition of overlapping atomic potentials. For the latter, we used relativistic self-consistent atomic potentials based on the Kohn-Sham version of the free-electron exchange approximation.[13,14] The present relativistic OPW band calculation for grey tin closely paralleled earlier calculations of this type for a number of tetrahedrally bonded semiconductors,[15] and for a number of IV-VI compounds.[16]

Our principal numerical results are listed in Table I. Here we show the energy eigenvalues for the four valence bands and the lowest six conduction bands at seven key points in the reduced zone. The zero of energy has been placed at the level Γ_8^+. Most of the levels are identified by their double group-symmetry symbols, as well as by the single group-symmetry species from which they are derived. We wish to emphasize that all of the numerical results in Table I are based on a first-principles band calculation, and involve no empirical corrections or adjustments of any kind.

All the levels at $\Lambda[\vec{k}=(\frac{1}{4},\frac{1}{4},\frac{1}{4})$, where $\vec{k}$ is in units of $2\pi/a$], L, $W[\vec{k}=(1,\frac{1}{2},0)]$, $\Delta[\vec{k}=(\frac{1}{2},0,0)]$, and $\Sigma[\vec{k}=(\frac{1}{2},\frac{1}{2},0)]$ are doubly degenerate, as are the $\Gamma_6^\pm$ and $\Gamma_7^\pm$ levels at Γ. All the levels at X and $\Gamma_8^\pm$ are fourfold degenerate. In the case of the W point, we did not go to the trouble of determining the double group-symmetry classification for the various levels. However, we know that $W_1 \rightarrow W_3 + W_5 + W_7$, that $W_2 \rightarrow W_4 + W_6 + W_7$, and that $W_3 = W_5$ and $W_4 = W_6$ by time-reversal symmetry.[17]

It will be noted that the order of levels at the zone center is precisely that envisioned in the Groves-Paul energy-band model,[18] i.e., the level derived from $\Gamma_{2'}^l$ lies between the spin-orbit split partners of $\Gamma_{25'}^l$. Our values for $\Gamma_8^+ - \Gamma_7^-$ (0.416 eV) and $\Gamma_8^+ - \Gamma_7^+$ (0.654 eV) are in reasonable agreement with experimental results.[18-20] The same can be said for the indirect band gap, $L_{6c}^+ - \Gamma_8^+$ (0.15 eV).[18] The magnitude and sign of this indirect band gap are fully consistent with the Groves-Paul energy-band model.

We note in passing that the present results are in good agreement with an earlier solution for grey tin, based on an empirically refined (nonrelativistic) OPW energy-band calculation.[21]

B. $\vec{k}\cdot\vec{p}$ Energy Bands

In the optical region the orbital electronic energy bands of diamond-type semiconductors can be calculated by a full-zone $\vec{k}\cdot\vec{p}$ technique using as a basis 15 orbital states referred to $\vec{k}=0$.[1] These states correspond to plane-wave states of wave vector [000], [111], and [200] and are labeled Γ_1^l, $\Gamma_{25'}^l$, $\Gamma_{2'}^l$, Γ_{15}, Γ_1^u, $\Gamma_{12'}$, $\Gamma_{25'}^u$, and $\Gamma_{2'}^u$ in Table I. The energies of these states, with the exception of the last two, were taken from the OPW values listed in Table I by correcting for the spin-orbit splittings. The energies of the remaining two levels were obtained by solving 2×2 pseudopotential matrices using the parameters of Cohen and Bergstresser.[22] It was found that the bands of interest are insensitive to the choice of values for $\Gamma_{25'}^u$ and $\Gamma_{2'}^u$.

Ten independent matrix elements of the momentum $\vec{p}$ between the above states are allowed by group theory. The values for these parameters listed in Table II were obtained in the following manner. Along Δ the energy of the highest-lying valence band depends only on Q and Q' and hence these parameters were adjusted until the $\vec{k}\cdot\vec{p}$ bands agreed with the OPW calculation at $\vec{k}=(\frac{1}{2},0,0)$ and at X. The doubly degenerate Λ_3 orbital bands depend on Q, Q', R, and R' so that once the former two parameters have been determined, the latter two were obtained by fitting the energies of the $L_{3'}$ valence and L_3 conduction bands (see Fig. 1).

Values for T and T' were arrived at by adjusting the Δ_{6c} conduction band and lowest-lying Δ_6 valence band (not shown in Fig. 1) at the edge of the zone (X_5) to the OPW energies listed in Table I. The matrix elements P, P', and P''' were then determined by arranging the Δ_{7c} conduction band and lowest-lying Δ_7 valence bands (not shown in Fig. 1) so that they were degenerate with the respective Δ_6 band at X, and by fitting the energy of the L_{6c}^+

TABLE II. Matrix elements of the linear momentum $\vec{p}$ (in atomic units) and spin-orbit splitting parameters (in eV) for α-Sn as obtained from the $\vec{k}\cdot\vec{p}$ method and experiment.

	Theory	Expt
$P(2i\langle\Gamma_{25'}^l\lvert\vec{p}\rvert\Gamma_{2'}^l\rangle)$	1.1281	1.33 (Ref. 20), 1.69 (Ref. 19)
$P'(2i\langle\Gamma_{25'}^u\lvert\vec{p}\rvert\Gamma_{2'}^u\rangle)$	0.1800	
$P''(2i\langle\Gamma_{25'}^l\lvert\vec{p}\rvert\Gamma_{2'}^u\rangle)$	0.0380	
$P'''(2i\langle\Gamma_{25'}^u\lvert\vec{p}\rvert\Gamma_{2'}^u\rangle)$	1.1145	
$Q\ (2i\langle\Gamma_{25'}^l\lvert\vec{p}\rvert\Gamma_{15}\rangle)$	0.9267	
$Q'\ (2i\langle\Gamma_{25'}^u\lvert\vec{p}\rvert\Gamma_{15}\rangle)$	−0.5868	
$R\ (2i\langle\Gamma_{25'}^l\lvert\vec{p}\rvert\Gamma_{12'}\rangle)$	0.7358	
$R'\ (2i\langle\Gamma_{25'}^u\lvert\vec{p}\rvert\Gamma_{12'}\rangle)$	1.1258	
$T\ (2i\langle\Gamma_1^u\lvert\vec{p}\rvert\Gamma_{15}\rangle)$	0.9523	
$T'\ (2i\langle\Gamma_1^l\lvert\vec{p}\rvert\Gamma_{15}\rangle)$	0.3560	
$\Delta_{25'}$	0.644	0.80 (Ref. 20)
Δ_{15}	0.479	
$\Delta_{25'}^{ul}$	0.556	

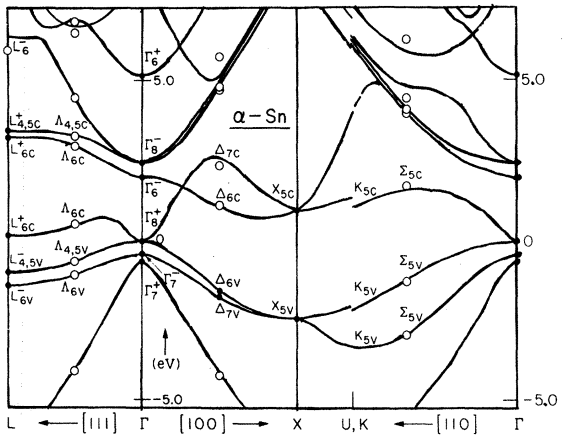

FIG. 1. Energy bands of α-Sn along Δ, Λ, Σ and the line joining X and U, K. The double group notation has been used to label the bands. The circles represent the values obtained from the OPW calculation; the closed circles indicate those energies used to fit the $\vec{k}\cdot\vec{p}$ parameters.

(in double group notation) conduction band. As in previous calculations for Ge, Si,[1] and α-Sn,[3] it was found that the bands of interest are insensitive to P'' and hence an approximate value was determined using the pseudopotential parameters mentioned before. In contrast to the OPW or pseudopotential methods which use symmetrized combinations of wave functions, those degeneracies which are required by the translational symmetry of the crystal are not incorporated into the full-zone $\vec{k}\cdot\vec{p}$ method and therefore the degeneracy at X must be imposed.

In previous full-zone calculations for diamond-type materials the eigenvectors of the orbital $\vec{k}\cdot\vec{p}$ Hamiltonian were used to determine the effects of the spin-orbit interaction using only two matrix elements of the spin-orbit Hamiltonian $\mathcal{H}_{so}$.[1-3] Thus

$$\begin{aligned}\Delta_{25'} &= (3i/c^2)\langle X(\Gamma^l_{25'})\uparrow|\mathcal{H}_{so}|Y(\Gamma^l_{25'})\uparrow\rangle\ ,\\ \Delta_{15} &= (3i/c^2)\langle x(\Gamma_{15})\uparrow|\mathcal{H}_{so}|y(\Gamma_{15})\uparrow\rangle\ ,\end{aligned} \tag{1}$$

where the notation is that of Ref. 1 and c is the speed of light. The choice of only these two parameters was dictated by the amount of available experimental evidence. Values for $\Delta_{25'}$ and Δ_{15} were determined from the experimentally observed spin-orbit splitting of the $\Gamma_{25'}$ valence band (Ge and Si) or the Λ_3 valence band (α-Sn) and the degeneracy imposed by symmetry at the X_{5v} valence-band state.[23] However, in the present work it is possible to consider more spin-orbit parameters. We have found the coupling between the upper and lower $\Gamma_{25'}$ states, $\Delta^{ul}_{25'}$, where

$$\Delta^{ul}_{25'} = (3i/c^2)\langle X(\Gamma^u_{25'})\uparrow|\mathcal{H}_{so}|Y(\Gamma^l_{25'})\uparrow\rangle \tag{2}$$

is approximately equal to $\Delta_{25'}$ and Δ_{15}. All other spin-orbit parameters which could affect the bands involved in optical transitions (e.g., the coupling between $\Gamma_{12'}$ and Γ_{15}) were found to be at least a factor of 2 smaller than the above three matrix elements and hence were neglected. Listed in Table II are the values of $\Delta_{25'}$, Δ_{15}, and $\Delta^{ul}_{25'}$ obtained by fitting the spin-orbit splitting of the $\Gamma_{25'}$ valence band and Γ_{15} conduction band listed in Table I and by imposing the degeneracy at X_{5v} (see Fig. 1).

Shown in Fig. 1 are the energy bands of α-Sn along Δ, Λ, and Σ as determined from the full-zone $\vec{k}\cdot\vec{p}$ method by diagonalizing a 30×30 matrix (including spin) using the parameters listed in Tables I and II. Also shown are the bands along the line joining X and U. The double group notation has been used to label the bands. The circles represent the values obtained from the OPW calculation; the closed circles indicate those energies which were used to fit the $\vec{k}\cdot\vec{p}$ parameters. Listed in Table I are all of the levels calculated by the OPW technique and the corresponding $\vec{k}\cdot\vec{p}$ values. Figure 1 and Table I indicate that throughout the entire zone the agreement is very good, from the lowest-lying valence bands up to about 6 eV. Above this energy there is good accord along Λ to L and along Δ to $\vec{k}\approx(\frac{1}{2},0,0)$, while at X, W, and Σ $[k=(\frac{1}{2},\frac{1}{2},0)]$ there are discrepancies of 1–2 eV. Since the optical constants have been determined to only 7 eV, the agreement is quite satisfactory with the possible exception of the W point where the OPW value is 4.03 eV while the $\vec{k}\cdot\vec{p}$ result is 9.14 eV.

A further indication of the reliability of the full-zone $\vec{k}\cdot\vec{p}$ method as an interpolation scheme is the fact that in the optical region the bands reach the edge of the zone with zero slope (or zero average slope) at those points required by crystal symmetry. In addition the points at U and K are almost degenerate with the exception of the conduction band along Σ originating from Γ_6^-. The reason that this band does not bend over near K (as indicated by the dotted lines in Fig. 1) is probably due to the fact that plane-wave states above [200] have been neglected. This is also the reason why the bands along Δ above 6 eV do not reach the edge of the zone with zero (or zero average) slope and the discrepancy at W mentioned above.

The bands shown in Fig. 1 are in good agreement with a recent pseudopotential calculation including spin-orbit interaction by Bloom and Bergstresser.[24] The main differences are in the spin-orbit splitting of the $\Gamma^l_{25'}$ valence band (0.73 eV in Ref. 24) and the energy separation between

the upper valence bands and the Γ_6^-, Γ_8^- levels. These authors find, for example, that the $\Gamma_6^- - \Gamma_8^+$ gap is 2.45 eV while we obtain a value of 1.96 eV.

From the eigenvectors of the $\vec{k}\cdot\vec{p}$ Hamiltonian, the matrix elements listed in Table II, and the energy gaps listed in Table I, we have calculated mass parameters at several points in the zone and g factors at Γ_7^- and Γ_7^+. These are listed in Table III together with available experimental data. The valence-band mass parameters F, G, H_1, and H_2 are those of Dresselhaus, Kip, and Kittel.[25] In our calculation of F we have omitted the interaction with Γ_2^u, since this contribution is negligible; hence (in atomic units),[26]

$$F = P^2/[E(\Gamma_7^-) - E(\Gamma_8^+)] \ . \tag{3}$$

Since we have not considered any Γ_{25} states, $H_2 = 0$. The parameter q, where (in atomic units)

$$q = 8|\langle \Gamma_{15}|p_y|X\rangle|^2 \Delta_{15}/9[E(\Gamma_8^+) - E(\Gamma_{15})]^2 \ , \tag{4}$$

was postulated by Luttinger[27]: It gives the effect of the spin-orbit splitting of Γ_{15} on the mass parameters of Γ_8^+. It has recently been measured in InSb by Pidgeon and Groves[28] and in Ge by Hensel and Suzuki.[29]

Our calculated value of F is somewhat lower than the experimental values. In the case of Groves *et al.*[19] this discrepancy is due to P (see Table II) since the calculated (0.416 eV) and experimental (0.413 eV) values for the $\Gamma_8^+ - \Gamma_7^-$ gap are in good agreement while in the case of Booth and Ewald[19] the difference is due to both parameters $[E(\Gamma_8^+) - E(\Gamma_7^-) = 0.63$ eV$]$. However, Booth and Ewald note that their values of both P and $E(\Gamma_8^+) - E(\Gamma_7^-)$ may be in error since the effects of some bands have been neglected in their analysis.

There is a serious disagreement for the quantity G. Both experiments give a positive value while the calculation gives a negative value. The $\Gamma_{12'}$ bands which contribute to the $\vec{k}\cdot\vec{p}$ sum for G derive from antibonding d-like levels. The negative calculated value occurs because only the $\Gamma_{12'}$ conduction band, with $5d$ character, has been considered. The positive experimental values of G indicate that the $4d$ valence bands (see Table I) must be taken into account.

The discrepancy for $m^*(\Gamma_7^-)$ is caused mainly by our somewhat low value for the spin-orbit splitting of the $\Gamma_{25'}^l$ valence band (see Table II). The expression for $m^*(\Gamma_7^-)$ is given by (neglecting interactions with higher-lying bands)

$$\frac{1}{m^*(\Gamma_7^-)} = 1 + \frac{P^2}{3}\left(\frac{2}{E(\Gamma_7^-) - E(\Gamma_8^+)} + \frac{1}{E(\Gamma_7^-) - E(\Gamma_7^+)}\right) . \tag{5}$$

Since in the above equation the energy denominators have opposite signs and are approximately equal, there is considerable cancellation between the two terms. A small error in these energies will thus have a large effect on the mass.

TABLE III. Calculated and experimental values of the band parameters (in units of free-electron mass) at Γ_8^+, Γ_7^-, Γ_7^+, the Δ_{6c} and the L_{6c}^+ conduction-band minima. Also listed are the g factors (in units of Bohr magnetons) at Γ_7^- and Γ_7^+.

	Theory	Expt
F	+41.6	+58.3[a], +65 ±2[b,c]
G	−1.89	+0.56[a], +3 ±0.1[b]
H_1	−5.15	−8.04[a], −8.0 ±0.4[b]
H_2	0	0[a,b]
q[d]	+0.241	+0.42[a]
$m^*(\Gamma_7^-)$	−0.39	−0.058[a]
$m^*(\Gamma_7^+)$	−0.039	−0.041[a]
$m_\parallel^*(\Delta_{6c})$	0.89	
$m_\perp^*(\Delta_{6c})$	0.086	
$m_\parallel^*(L_{6c}^+)$	1.35	
$m_\perp^*(L_{6c}^+)$	0.072	
g (Γ_7^-)	−78.1	
g (Γ_7^+)	−48.9	

[a] See Ref. 20.
[b] See Ref. 19.
[c] In Ref. 19 this quantity is denoted by F'.
[d] See Refs. 27–29.

III. DETERMINATION OF OPTICAL CONSTANTS

The contribution of direct interband transitions to $\epsilon_2(\omega)$, the imaginary part of the complex dielectric constant, is given by (in atomic units)[30]

$$\epsilon_2(\omega) = \frac{4}{\pi\omega^2}\sum_{ij}\int_{Bz} d^3k\ |M_{ij}(\vec{k})|^2 \delta(\omega_{ij} - \omega) \ , \tag{6}$$

where $M_{ij}(\vec{k}) = \langle i|\vec{p}\cdot\hat{e}|j\rangle$ is the matrix element of the momentum $\vec{p}$ between occupied and empty states (i and j, respectively), $\hat{e}$ is the unit polarization vector of the incident radiation, and the integral is over the Brillouin zone (Bz). The method used to evaluate this integral was first applied to the calculation of phonon frequency distribution functions by Gilat *et al.*[10] In this technique the irreducible section of the zone ($\frac{1}{48}$ of the Bz) is divided into a uniform simple cubic mesh $\vec{k}_c$. Within each of these cubes the constant energy surfaces are approximated by sets of parallel planes perpendicular to $\nabla_{\vec{k}}\omega_{ij}(\vec{k}_c)$. The integral of Eq. (6) then reduces to an integral over constant energy planes within each cube; thus,

$$\epsilon_2(\omega) = \frac{4}{\pi\omega^2}\sum_{\vec{k}_c} W(\vec{k}_c)\sum_{ij}\int_{S_{ij}(w)} ds\ \frac{|M_{ij}(\vec{k}_c)|^2}{|\nabla_{\vec{k}}\omega_{ij}(\vec{k}_c)|} \ , \tag{7}$$

where $S_{ij}(w)$ is the area of the cross section of the cube for a plane located a distance w from $\vec{k}_c$, and $W(\vec{k}_c)$ is a weighting factor which is used because the cubic mesh does not exactly fill the volume of

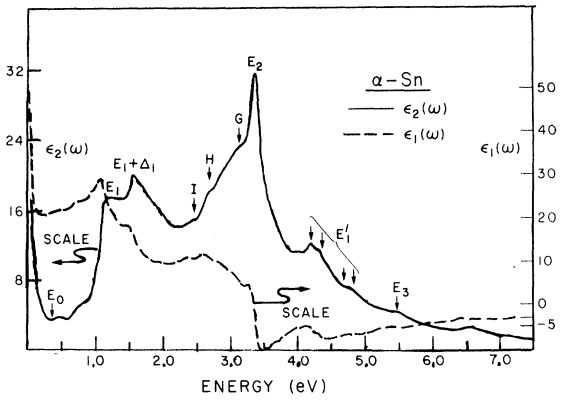

FIG. 2. Calculated values of the real $[\epsilon_1(\omega)]$ and imaginary $[\epsilon_2(\omega)]$ parts of the complex dielectric constant.

the irreducible section. $|M_{ij}(\vec{k})|^2$ is considered to be constant throughout the cube. The area is a polynomial of order 2 or less in w, and hence Eq. (7) can be integrated exactly between ω and $\omega+d\omega$ to yield a histogram for $\epsilon_2(\omega)$. In our case the distance in $\vec{k}$ space between centers of adjacent cubes was chosen to be $\pi/6a$, which is $\frac{1}{12}$ the distance between Γ and X. This choice was dictated by considerations of the time necessary to diagonalize the 30×30 $\vec{k}\cdot\vec{p}$ matrix. In order to obtain better resolution of the optical constants a finer mesh was obtained by expanding the energy to second order in $\vec{k}$ and evaluating the expansion coefficients from the eigenvectors of the $\vec{k}\cdot\vec{p}$ Hamiltonian at the center of the "coarse" cube using nondegenerate perturbation theory.[31] The distance between the constant energy surfaces and hence the resolution was set at 0.01 eV. A constant broadening parameter of 0.03 eV was introduced phenomenologically in order to smooth the curves.[31]

Shown in Fig. 2 are the calculated values of $\epsilon_1(\omega)$ and $\epsilon_2(\omega)$, the real and imaginary parts of the complex dielectric constant, respectively, where $\epsilon_1(\omega)$ was obtained by a Kramers-Kronig analysis of $\epsilon_2(\omega)$. Plotted in Fig. 3 are $n(\omega)$ and $k(\omega)$, the real and imaginary parts of the complex index of refraction, respectively. The calculated and experimental[32] values of the normal incidence reflectivity (R) in the energy range 0–5 eV are shown in Fig. 4. At the bottom of the figure we have indicated by arrows the positions of structure seen in electroreflectance.[4,32] Comparison of the reflectivity rather than $\epsilon_2(\omega)$ is made since R has not been measured in a sufficiently large energy range to obtain reliable values of $\epsilon_2(\omega)$.

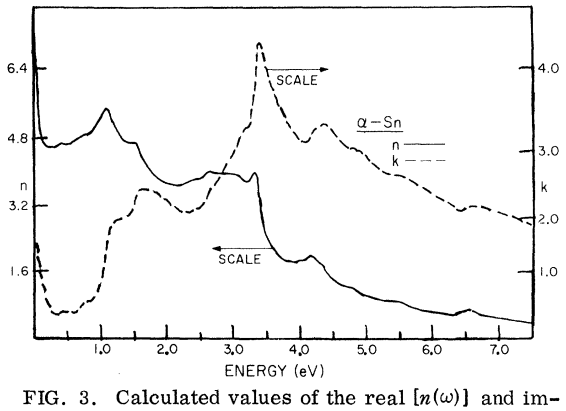

FIG. 3. Calculated values of the real $[n(\omega)]$ and imaginary $[k(\omega)]$ parts of the complex index of refraction.

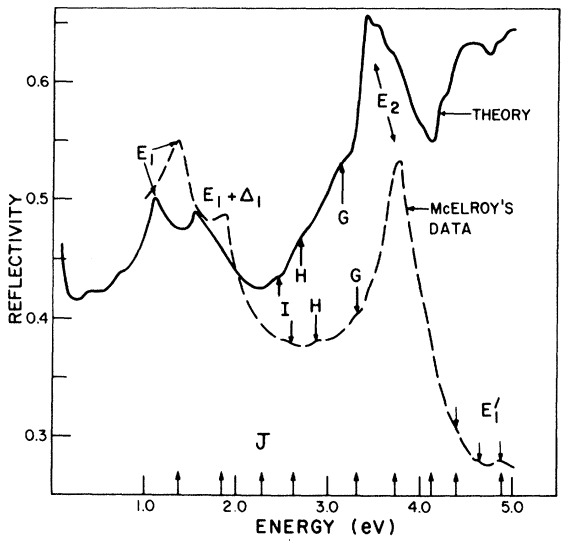

FIG. 4. Calculated and experimental (Ref. 12) values of the normal incidence reflectivity in the range 0–5 eV. The arrows at the bottom of the figure indicate the positions of the structure seen in electroreflectance (Refs. 4 and 32).

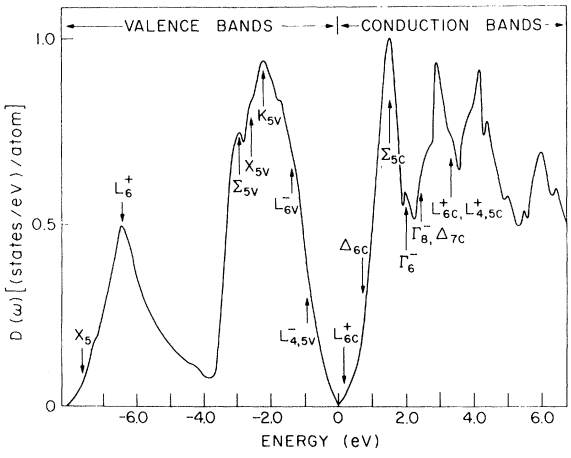

FIG. 5. Individual electronic density of states for the upper three valence bands (six including spin) and lower three conduction bands of α-Sn.

The individual electronic density of states, $D(\omega)$, for the upper three valence bands and lower three conduction bands is plotted in Fig. 5.

IV. COMPARISON OF EXPERIMENTAL AND CALCULATED REFLECTIVITY

The over-all features of the calculated R are in reasonably good agreement with McElroy's data. There is a difference of 0.2-0.3 eV in the positions of the structure. This discrepancy could be corrected by slightly revising the OPW calculation. There is some difference in the line shape of the E_1 doublet which is caused by excitonic effects. This point will be discussed later. The disagreement in the intensity of the E_2 structure is probably due to experimental difficulties. In all the diamond- and zinc-blende-type materials the magnitude of E_2 is greater than the E_1 doublet in R.[5,33] However, if the surface of the sample is poor, E_2 is found to be smaller than E_1, as in Fig. 4. The low amplitude of E_2 has also made it impossible to reliably determined $\epsilon_2(\omega)$ from the experimental R.

At energies above E_2 there is a sharp decrease in the experimental curve, with some structure labeled E_1', while an increase is observed in the calculated curve. This discrepancy is probably due to (a) the truncation at 10 eV of the Kramers-Kronig analysis used to generate $\epsilon_1(\omega)$ from $\epsilon_2(\omega)$, and (b) the difficulty with the bands above 6 eV as discussed in Sec. II B. Similar difficulty above E_2 has been encountered by Walter and Cohen[34] in a pseudoptential calculation of serveral cubic semiconductors even though they have used an analytic tail in $\epsilon_2(\omega)$ above about 9 eV.

In order to identify the origins of the structure in the optical spectrum we have also calculated (a) the contributions to the total $\epsilon_2(\omega)$ from six

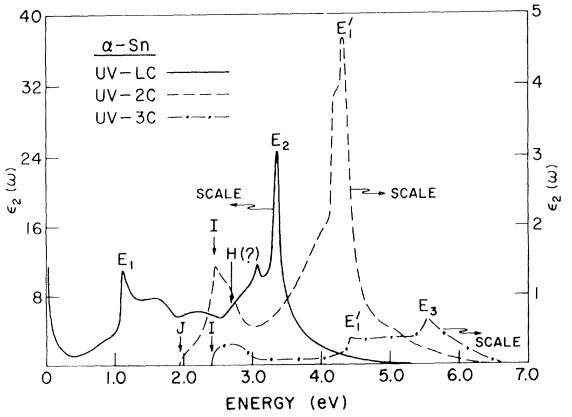

FIG. 6. Contributions to $\epsilon_2(\omega)$ due to transitions from the upper valence band (UV) to the lowest (LC), second (2C), and third (3C) conduction bands.

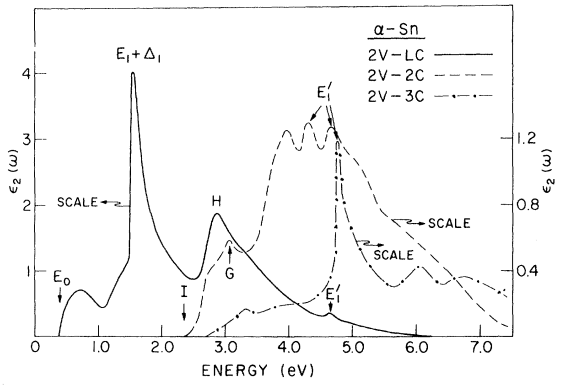

FIG. 7. Contributions to $\epsilon_2(\omega)$ due to transitions from the second valence band (2V) to the lowest (LC), second (2C), and third (3C) conduction bands.

pairs of bands, (b) the constant energy contours for these transitions in the (110) plane (most of the important symmetry points and lines lie in this plane), and (c) the derivative optical constants $d\epsilon_1/d\omega$, $d\epsilon_2/d\omega$, and $R^{-1}\,dR/d\omega$. Shown in Fig. 6 are the contributions to $\epsilon_2(\omega)$ due to transitions from the upper valence band (UV) to the lowest (LC), second (2C), and third (3C) conduction bands. It should be noted that at $\vec{k} \approx (\frac{1}{4}, 0, 0)$ the lowest-lying conduction band changes from Δ_{7c} to Δ_{6c} (see Fig. 1). Plotted in Fig. 7 are the contributions from the second valence band (2V) to the three conduction bands. No broadening has been introduced in these calculations. The constant energy contours for these six transitions are shown in Figs. 8–13. The derivative optical constants are displayed in Fig. 14.

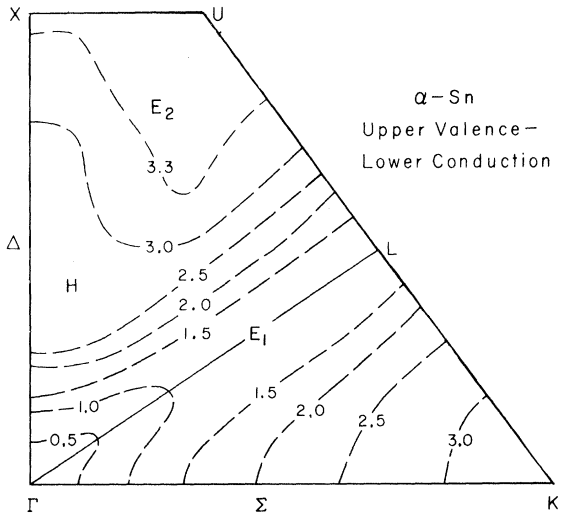

FIG. 8. Constant energy contours (in eV) of the UV-LC transition in the (110) plane.

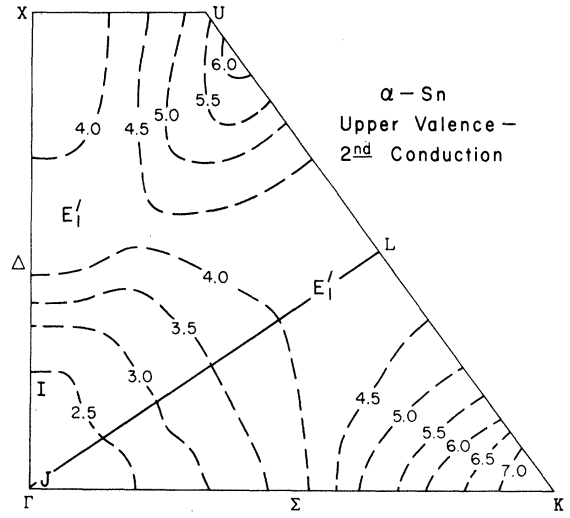

FIG. 9. Constant energy contours (in eV) of the UV-2C transition in the (110) plane.

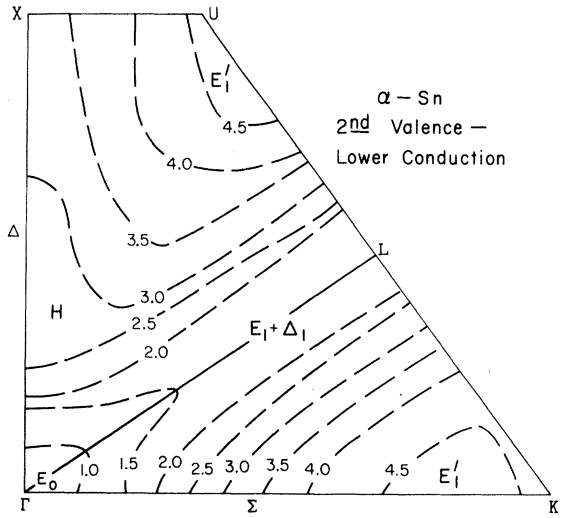

FIG. 11. Constant energy contours (in eV) of the 2V-LC transition in the (110) plane.

The first structure seen in the experimental reflectivity is the E_1, $E_1+\Delta_1$ doublet, which occurs at energies of 1.365 and 1.832 eV, respectively. The corresponding peaks in the calculated $\epsilon_2(\omega)$ and R (see Figs. 2 and 4) occur at somewhat lower values of 1.1 and 1.55 eV. A similar structure has been observed in the optical spectra of all of the diamond- and zinc-blende-type semiconductors except Si.[5, 32] Uniaxial stress measurements on a number of these materials[35–37] have shown that the doublet corresponds to transitions between the spin-orbit split Λ_3 valence band (in single group notation) and the lowest-lying Λ_{6c} conduction band. An analysis of the individual $\epsilon_2(\omega)$ and constant energy contours reveals that the calculated doublet arises from UV-LC and 2V-LC transitions along Λ from $\vec{k} \approx (\frac{1}{6}, \frac{1}{6}, \frac{1}{6})$ to L. These are labeled E_1 in Fig. 8 and $E_1+\Delta_1$ in Fig. 11. The line shapes of $\epsilon_2(\omega)$ and $d\epsilon_2/d\omega$ indicate that these gaps are of the M_1- or two-dimensional minima type.[30, 33, 38, 39] In Fig. 15 we have plotted $\epsilon_2(\omega)$ in the vicinity of a Van Hove singularity[38] in one, two, and three dimensions assuming a constant matrix element. The discrepancy between the theoretical and experimental line shapes is due to excitonic effects, which have not been included in the calculation. The existence of excitons at a hyperbolic (M_1) critical point has been demonstrated by studying the stress-induced exchange splitting of the E_1,

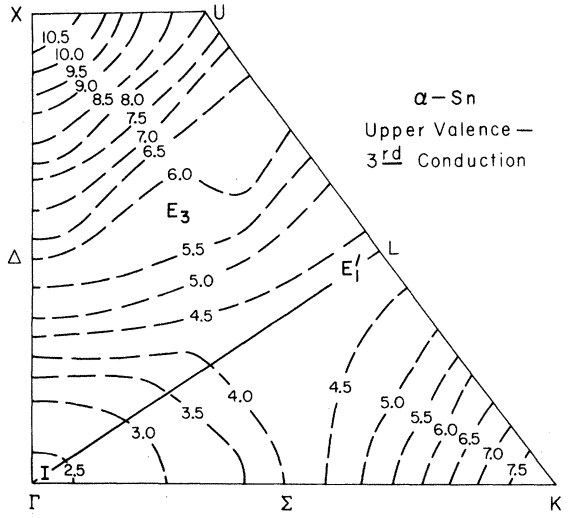

FIG. 10. Constant energy contours (in eV) of the UV-3C transition in the (110) plane.

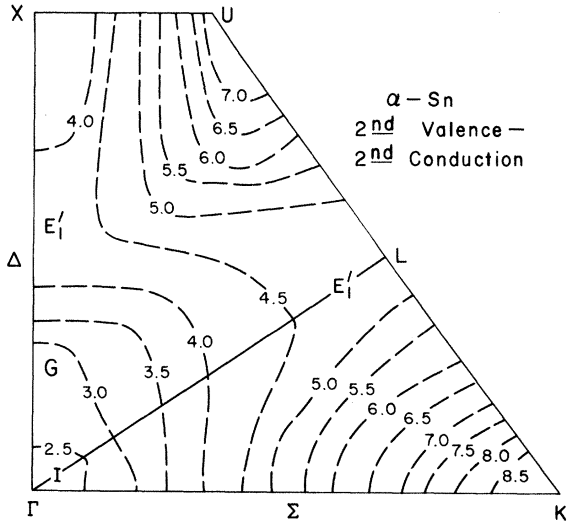

FIG. 12. Constant energy contours (in eV) of the 2V-2C transition in the (110) plane.

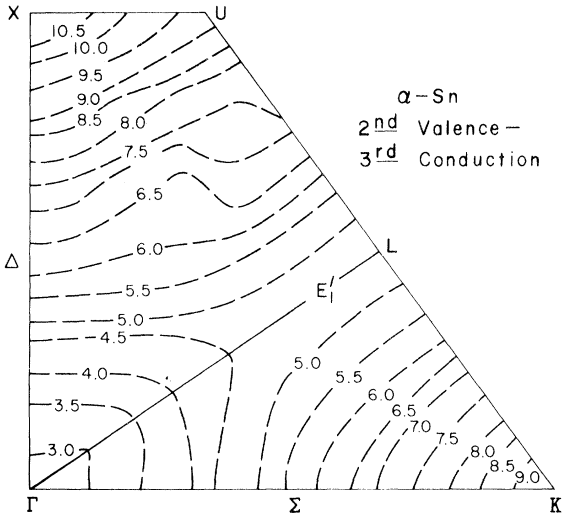

FIG. 13. Constant energy contours (in eV) of the 2V-3C transition in the (110) plane.

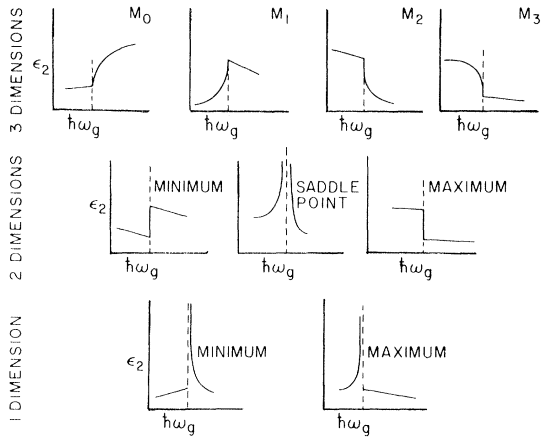

FIG. 15. Imaginary part of the complex dielectric constant, $\epsilon_2(\omega)$, in the vicinity of a Van Hove singularity in one, two, and three dimensions, assuming a constant matrix element. The energy of the gap is given by $\hbar\omega_g$.

$E_1+\Delta_1$ structure in GaAs.[40] Analysis of the wavelength-derivative spectrum of this doublet in InSb has shown that the electron-hole interaction at an M_1 critical point results in a mixing of M_1 and M_2 line shapes.[41] Such an admixture would change the line shape of the calculated R from peaks which are approximately symmetrical about their maxima to ones having a more abrupt high-energy side, thus bringing the two curves into better agreement.

In the energy region 2–3 eV four structural features are observed experimentally between the strong peaks associated with the E_1 doublet and E_2. There is structure in electroreflectance at 2.28 eV, at about 2.6 eV in both reflectivity and electroreflectance, 2.85 eV in reflectivity only, and at about 3.3 eV in both R and electroreflectance. Following McElroy[12] we have labeled these J, I, H, and G, respectively. In Refs. 4 and 32, J and I have been denoted by E_0' and $E_0'+\Delta_0'$, respectively. The calculated curves for $\epsilon_2(\omega)$ and R have shoulders at 2.45, 2.7, and 3.15 eV. There is also structure in the theoretical values of $d\epsilon_2/d\omega$ and $R^{-1}\,dR/d\omega$ at about these energies. Since the calculated values of the E_1 doublet and the E_2 peak are approximately 0.2 eV lower than experiment, it seems reasonable to associate these three calculated structural features with I, H, and G and to look for the origins of J at about 2 eV. Inspection of the individual $\epsilon_2(\omega)$ shows that there is a square-root edge (M_0) at 1.96 eV caused by UV-2C transitions at $\vec{k}=0(\Gamma_6^- - \Gamma_8^+)$. The absence of this edge in the total $\epsilon_2(\omega)$ and reflectivity is not surprising since it is very weak and would be superimposed on the high-energy side of the large $E_1+\Delta_1$ peak. However, M_0 critical points show up strongly in electroreflectance and hence the J spectral feature should be ascribed to the $\Gamma_6^- - \Gamma_8^+$ transitions. With regard to the I structure Figs. 6 and 7 indicate three possible sources. There is a strong peak in the UV-2C curve at 2.45 eV which has an M_1- or two-dimensional minima-type line shape (see Fig. 15). The constant energy contour shows that these bands are fairly flat along Δ near Γ (I in Fig. 9) with approximately this energy separation and hence it is probably this region that causes the peak in the individual $\epsilon_2(\omega)$. Based on an earlier OPW calculation by Herman *et al.*,[21] McElroy has also identified I with $\Delta_{6c}-\Delta_{6v}$ transitions. Figure 6 also shows a weak contribution from UV-3C transitions starting at about 2.4 eV,

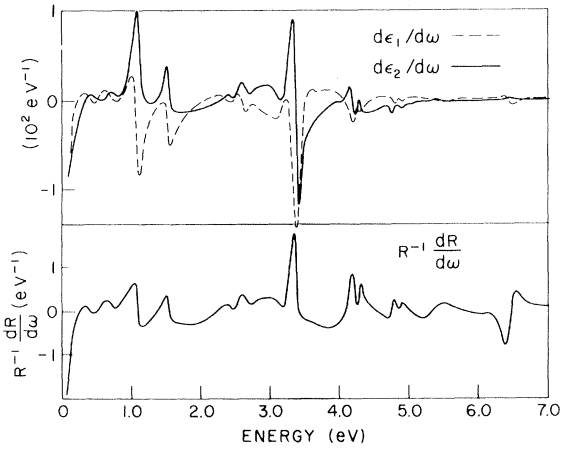

FIG. 14. Calculated derivative optical constants $d\epsilon_1/d\omega$, $d\epsilon_2/d\omega$, and $R^{-1}\,dR/d\omega$.

which corresponds to the $\Gamma_8^- - \Gamma_8^+$ gap. Figure 7 indicates that the $\epsilon_2(\omega)$ contribution from 2V-2C transitions begin at about 2.4 eV. At $\vec{k}=0$ this transition ($\Gamma_6^- - \Gamma_7^-$) is forbidden in reflectivity because of parity, but becomes allowed off Γ and hence $\epsilon_2(\omega)$ has a three-halves power line shape near the gap. McElroy has indicated that the $\Gamma_6^- - \Gamma_7^-$ transition is allowed in electroreflectance since the electric field lifts the parity selection rule. Thus it is possible that the $\Gamma_6^- - \Gamma_7^-$ transition gives the dominant contribution to the electroreflectance spectrum at 2.6 eV while the $\Delta_{6c} - \Delta_{6v}$ transitions produce the I reflectivity shoulder. These results are summarized in Table IV.

Contributions to the spectral feature H may also come from several sources. There is a shoulder in the $\epsilon_2(\omega)$ of UV-LC starting at about 2.6 eV (see Fig. 6). The contours are quite flat with this energy separation in the region labeled H in Fig. 8 (in this region the conduction bands have already crossed so the transition is $\Delta_{6c} - \Delta_{6v}$). In addition, there is a fairly strong peak in the 2V-LC curve at 2.8 eV also originating from transitions near $\vec{k} \approx (\frac{1}{3}, 0, 0)$. These $\Delta_{6c} - \Delta_{7v}$ transitions have been labeled H in Fig. 11.

In the UV-LC curve (Fig. 6) there is a sharp peak at 3.1 eV which might presumably be associated with the calculated G spectral structure. However, this peak is spurious owing to the fact that U and K are not degenerate. If the degeneracy were imposed this peak would merge with the large E_2 structure and hence we must look elsewhere for the origins of the experimental G structure. Table I and Fig. 1 reveal that the energy of the $\Gamma_8^- - \Gamma_7^+$ gap is 3.1 eV. This transition has been included in the total $\epsilon_2(\omega)$ of Fig. 2 although we have not calculated the individual $\epsilon_2(\omega)$. Another possibility is 2V-2C transitions along Δ near Γ (G in Fig. 12).

The E_2 reflectivity peak appears as the main spectral structure of most diamond- and zinc-blende-type materials.[5, 32] As mentioned before the discrepancy in the amplitude between the calculated and measured curves is probably due to a poor surface. In Ge and Si E_2 was originally assigned to $X_{5c} - X_{5v}$ transitions possibly combined with transitions at a Σ saddle point (Σ_{5c}-upper Σ_{5v}) on the basis of a suggestion by Phillips[3] and later pseudopotential calculations by Brust.[42] Piezoreflectivity measurements on Ge and Si[35] provide some evidence for the X assignment although they are by no means conclusions. Electroreflectance studies in Si[32] show a structure on E_2 which may be caused by the Σ transitions. The band calculations of Herman *et al.*[21] for Ge and Si and Kane[43] for Si indicate that the assignment of this structure to only X and Σ critical points

TABLE IV. Comparisons of the energies (in eV) of experimental and theoretical optical structure. Also indicated are the transitions responsible for the structure in the calculated spectrum.

Spectral feature	Experiment		Theory	
	Reflectivity[a]	Electroreflectance[b]	Energy	Transition
E_0	c		0.4	$\Gamma_8^+ - \Gamma_7^-$
E_1	1.365	1.365	1.10	$\Lambda_{6c} - \Lambda_{4,5v}$
$E_1 + \Delta_1$	1.832	1.845	1.55	$\Lambda_{6c} - \Lambda_{6v}$
J		2.28	1.96	$\Gamma_6^- - \Gamma_8^+$
I	2.62	2.63	2.45	$\Delta_{6c} - \Delta_{6v}$ (near Γ)
				$\Gamma_8^- - \Gamma_8^+$ (weak)
				$\Gamma_6^- - \Gamma_7^-$[d]
H	2.85		2.7	$\Delta_{6c} - \Delta_{7v}$[e]
				$\Delta_{6c} - \Delta_{6v}$[e] (?)
G	3.3	3.3	3.15	$\Gamma_8^- - \Gamma_7^+$ (?)
				$\Delta_{6c} - \Delta_{7v}$[f]
E_2	3.75	3.718	3.35	UV-LC around X-U, K
E_1'	4.0	4.12	4.2	$L_{6c}^+ - L_{4,5v}^-$[g]
				$\Delta_{7c} - \Delta_{6v}$[e]
	4.43	4.43	4.4	$L_{4,5c}^+ - L_{4,5v}^-$[g]
				$\Delta_{7c} - \Delta_{7v}$[e]
	4.66		4.65	$L_{6c}^+ - L_{6v}^-$[g]
				UV-2C around U and K
	4.88	4.89	4.8	$L_{4,5c}^+ - L_{6v}^-$[g]
E_3			5.4	UV-3C

[a] See Ref. 12.

[b] See Refs. 4 and 32.

[c] Magnetoreflection studies have yielded a value of 0.413 eV (see Ref. 20).

[d] Allowed in electroreflectance only.

[e] In region around $\vec{k} \approx (\frac{1}{2}, 0, 0)$.

[f] In region around $\vec{k} \approx (\frac{1}{5}, 0, 0)$.

[g] Also along Λ near L.

may be an oversimplification and that transitions in an extended region of the zone contribute to it. For GaAs Walter and Cohen[34] conclude that E_2 is caused almost entirely by $\Sigma_{5v} - \Sigma_{5c}$ transitions in the vicinity of $\vec{k} = (\frac{1}{1.7}, \frac{1}{1.7}, 0)$ with some contribution from $\Delta_5 - \Delta_1$ and $X_5 - X_1$ transitions (in single group notation). Based on the earlier α-Sn band calculation by Herman *et al.*[21] McElroy has attributed this structure to $\Delta_{7c} - \Delta_{7v}$ and $\Delta_{7c} - \Delta_{6v}$ transitions. In the present investigation we find that E_2 is caused almost entirely by UV-LC transitions (see Fig. 6). The constant energy contours for this transition indicates that there is a large region around X and U that contributes to this peak (E_2 in Fig. 8). Similar results have been obtained for InSb,[6, 31] which has a band structure quite similar to α-Sn in this region. The discrepancy in the line shape of Fig. 4 is probably due to computational difficulties. As mentioned before, above 4 eV the calculated reflectivity amplitude is too high thus pulling up the high-energy side of E_2. In the case of InSb, where it was possible to make a comparison of $\epsilon_2(\omega)$ rather than R, the calculated and experimental line shapes of the E_2 peak are in good agreement.[6, 31]

Above the E_2 peak there are three weak spectral features labeled E_1' in the experimental R at 4.43, 4.66, and 4.88 eV. McElroy also reports very weak structure at 4.0 eV. Structure in electro-

reflectance has been observed at 4.12, 4.43, and 4.88 eV, as indicated by the arrows at the bottom of the figure. Similar structure has been observed in most of the diamond- and zinc-blende-type semiconductors and is attributed to transitions between the spin-orbit split L_3 (Λ_3) conduction and $L_{3'}$ (Λ_3) valence bands.[5,33] This assignment was made on the basis of the observed equality between the splitting of two of the E_1' peaks and Δ_1, the spin-orbit splitting of the L_3 (or Λ_3) valence band. Although no corresponding structure appears in the calculated R, four weak peaks are observable in $\epsilon_2(\omega)$ (see Fig. 2) at energies of 4.2, 4.4, 4.6, and 4.8 eV, which correspond to the gaps of the spin-orbit split $L_{3'}$ valence (L_{6v}^- and $L_{4,5v}^-$) and L_3 conduction (L_{6c}^+ and $L_{4,5c}^+$) bands. Examination of Fig. 6 shows a strong peak with a shoulder on the low-energy side at about 4.3 eV in the UV-2C curve. The constant energy contour of this transition (Fig. 9) reveals that these bands are quite flat in this energy region near L ($L_{6c}^+ - L_{4,5v}^-$) along Λ and that there is an M_1 critical point due to the maxima in Δ_{7c} at $\vec{k} \approx (\frac{1}{2}, 0, 0)$. Figure 6 also shows structure in the UV-3C curve at 4.4 eV which corresponds to $L_{4,5c}^+ - L_{4,5v}^-$ transitions (see Fig. 10). The difference in amplitude between UV-2C and UV-3C is caused mainly by a difference in M_{ij} [see Eqs. (6) and (7)]. In the 2V-2C curve there are three small peaks at 4.0, 4.3, and 4.65 eV. Examination of the constant energy contours of Fig. 12 reveals that the latter structure is due to $L_{6c}^+ - L_{6v}^-$ (and nearby Λ) transitions while the 4.3-eV structure comes from $\Delta_{7c} - \Delta_{7v}$ in the region of the zone where Δ_{7c} has a maximum (see Fig. 1). We have not been able to identify the origin of the 4.0-eV peak since the bands are fairly flat at this energy at a number of points of the zone. In addition there is a small spectral feature in the 2V-LC curve at about 4.65 eV which comes from the regions of the zone marked E_1' in Fig. 11. In the individual $\epsilon_2(\omega)$ for the 2V-3C transitions (Fig. 7) there is a sharp peak at 4.8 eV which is due to $L_{4,5c}^+ - L_{6v}^-$ transitions (see Fig. 13).

Above the E_1' spectral features a small peak labeled E_3 at about 5.5 eV appears in the calculated $\epsilon_2(\omega)$ in Fig. 2. This is caused by UV-3C transition in the region of the zone labeled E_3 in Fig. 10.

In the energy range below 1 eV there are two dominant features in the calculated $\epsilon_2(\omega)$ and R: the shoulder at 0.4 eV labeled E_0 and the rapid increase in these optical constants below this energy. As shown in Fig. 7, E_0 is due to 2V-LC transitions and corresponds to the $\Gamma_8^+ - \Gamma_7^-$ gap. Below this energy $\epsilon_2(\omega)$ is caused by only UV-LC transitions. Since the direct gap is zero $\epsilon_2(\omega)$ increases rapidly as ω approaches zero [see Eqs. (6) and (7)]. Because broadening has been included in the total $\epsilon_2(\omega)$ but not in the individual $\epsilon_2(\omega)$ there is a difference between Figs. 2 and 6 below E_0.

ACKNOWLEDGMENTS

We wish to thank Dr. S. H. Groves of Lincoln Laboratory and Dr. C. R. Pidgeon of the Francis Bitter National Magnet Laboratory for many useful discussions.

---

*Work supported by the National Science Foundation, the Advanced Research Projects Agency, and the Army Research Office, Durham, N. C.

†Present address: General Telephone and Electronics Laboratories, Bayside, N. Y.

‡Present address: Sandia Laboratory, Albuquerque, N. M.

[1]M. Cardona and F. H. Pollak, Phys. Rev. 142, 530 (1966); J. Phys. Chem. Solids 27, 423 (1966).

[2]M. Cardona, F. H. Pollak, and J. G. Broerman, Phys. Letters 19, 276 (1965).

[3]F. H. Pollak, C. W. Higginbotham, and M. Cardona, J. Phys. Soc. Japan Suppl. 21, 20 (1966).

[4]M. Cardona, P. McElroy, F. H. Pollak, and K. L. Shaklee, Solid State Commun. 4, 319 (1966).

[5]F. H. Pollak, in *Proceedings of the International Conference on II-VI Semiconducting Compounds*, 1967, edited by D. G. Thomas (Benjamin, New York, 1968), p. 552.

[6]C. W. Higginbotham, F. H. Pollak, and M. Cardona, in *Proceedings of the Ninth International Conference on the Physics of Semiconductors*, edited by S. M. Ryvkin (Nauka Publishing House, Leningrad, 1968), Vol. I, p. 57.

[7]C. W. Higginbotham, F. H. Pollak, and M. Cardona, Solid State Commun. 5, 513 (1967). Because of computational error, $\epsilon_2(\omega)$ for α-Sn above 4 eV is incorrect in this paper.

[8]W. Brinkman and B. Goodman, Phys. Rev. 149, 596 (1966).

[9]D. D. Buss and N. J. Parada, Bull. Am. Phys. Soc. 14, 29 (1969).

[10]G. Gilat and G. Dolling, Phys. Letters 8, 304 (1964); G. Gilat and L. J. Raubenheimer, Phys. Rev. 144, 390 (1966); L. J. Raubenheimer and G. Gilat, *ibid.* 175, 1156 (1968); G. Gilat and Z. Kam, Phys. Rev. Letters 22, 715 (1969).

[11]F. Herman, R. L. Kortum, C. C. Kuglin, and J. L. Shay, in Ref. 5, p. 503.

[12]P. T. McElroy, Technical Report No. HP-21 (ARPA-

34), Division of Engineering and Applied Physics, Harvard University, 1968 (unpublished).

[13]D. Liberman, J. T. Waber, and D. T. Cromer, Phys. Rev. 137, A27 (1965); see also Refs. 15 and 16.

[14]W. Kohn and L. J. Sham, Phys. Rev. 140, A113 (1965); see also Refs. 15 and 16.

[15]F. Herman, R. L. Kortum, C. D. Kuglin, J. P. Van Dyke, and S. Skillman, Methods Comput. Phys. 8, 193 (1968).

[16]F. Herman, R. L. Kortum, I. B. Ortenburger, and J. P. Van Dyke, J. Phys. (Paris) Colloq. 29, C4–62 (1968).

[17]R. J. Elliot, Phys. Rev. 96, 280 (1954).

[18]S. Groves and W. Paul, in *Proceedings of the International Conference on the Physics of Semiconductors, Paris*, 1964 (Dunod, Paris, 1964), p. 41; Phys. Rev. Letters 11, 194 (1963).

[19]B. L. Booth and A. W. Ewald, Phys. Rev. 168, 796 (1968); 168, 805 (1968).

[20]S. H. Groves, C. R. Pidgeon, A. W. Ewald, and R. J. Wagner, in Ref. 6, Vol. I, p. 43; J. Phys. Chem. Solids (to be published).

[21]F. Herman, R. L. Kortum, C. D. Kuglin, and R. A. Short, in *Quantum Theory of Atoms, Molecules, and the Solid State*, edited by P. O. Löwdin (Academic, New York, 1966), p. 381; J. Phys. Soc. Japan Suppl. 21, 7 (1966).

[22]M. L. Cohen and T. K. Bergstresser, Phys. Rev. 141, 789 (1966).

[23]Because of this degeneracy requirement $\Delta_{25'}$ and Δ_{15} are not independent.

[24]S. Bloom and T. K. Bergstresser, Solid State Commun. 6, 465 (1968).

[25]G. Dresselhaus, A. F. Kip, and C. Kittel, Phys. Rev. 98, 368 (1955).

[26]In these units the unit of length is the Bohr radius, $\hbar$ is the unit of action, and the Rydberg (1 Ry = 13.6 eV) is the unit of energy. In these fundamental units the unit of mass is $\frac{1}{2}$ the free-electron mass and the charge of the electron $e = \sqrt{2}$.

[27]J. M. Luttinger, Phys. Rev. 102, 1030 (1956).

[28]C. R. Pidgeon and S. H. Groves, Phys. Rev. 186, 824 (1969).

[29]J. C. Hensel and K. Suzuki, Phys. Rev. Letters 22, 838 (1969).

[30]See, for example, M. Cardona, in *Solid State Physics, Nuclear Physics, and Particle Physics*, edited by I. Saavedra (Benjamin, New York, 1968), p. 737.

[31]C. W. Higginbotham, Ph.D. thesis, Brown University, 1969 (unpublished).

[32]M. Cardona, K. L. Shaklee, and F. H. Pollak, Phys. Rev. 154, 696 (1967).

[33]See, for example, J. C. Phillips, in *Solid State Physics*, edited by F. Seitz and D. Turnbull (Academic, New York, 1966), Vol. 18, p. 55.

[34]J. P. Walter and M. L. Cohen, Phys. Rev. 183, 763 (1969).

[35]U. Gerhardt, Phys. Rev. Letters 15, 401 (1965); Phys. Status Solidi 11, 801 (1965).

[36]F. H. Pollak, M. Cardona, and K. L. Shaklee, Phys. Rev. Letters 16, 942 (1966).

[37]F. H. Pollak and M. Cardona, Phys. Rev. 172, 816 (1968).

[38]L. Van Hove, Phys. Rev. 89, 198 (1953).

[39]M. Cardona, in *Solid State Physics* (Academic, New York, 1969), Suppl. 11.

[40]J. E. Rowe, F. H. Pollak, and M. Cardona, Phys. Rev. Letters 22, 933 (1969).

[41]K. L. Shaklee, J. E. Rowe, and M. Cardona, Phys. Rev. 174, 828 (1968).

[42]D. Brust, Phys. Rev. 134, A137 (1964).

[43]E. O. Kane, Phys. Rev. 146, 558 (1966).